

Discrete Hyperbolic Random Graph Model

Dorota Celińska-Kopczyńska, Eryk Kopczyński

Institute of Informatics, University of Warsaw

September 27, 2021

Abstract

The hyperbolic random graph model (HRG) has proven useful in the analysis of scale-free networks, which are ubiquitous in many fields, from social network analysis to biology. However, working with this model is algorithmically and conceptually challenging because of the nature of the distances in the hyperbolic plane. In this paper, we propose a discrete variant of the HRG model where nodes are mapped to the vertices of a triangulation; our algorithms allow us to work with this model in a simple yet efficient way. We present experimental results conducted on networks, both real-world and simulated, to evaluate the practical benefits of DHRG in comparison to the HRG model.

Hyperbolic geometry has been discovered by the 19th century mathematicians wondering about the nature of parallel lines. One of the properties of this geometry is that the amount of an area in the distance d from a given point is exponential in d ; intuitively, the metric structure of the hyperbolic plane is similar to that of an infinite binary tree, except that each vertex additionally connects to two adjacent vertices on the same level.

Recently, hyperbolic geometry has proven useful in modeling hierarchical data [LRP95, Mun98]. In particular, it has found application in the analysis of scale-free networks, which are ubiquitous in many fields, from network analysis to biology [PKS⁺12]. In the hyperbolic random graph model (HRG), we place the nodes randomly in a hyperbolic disk; closer nodes are more likely to be connected. The properties of a HRG, such as its power-law degree distribution or high clustering coefficient, are similar to those of real-world scale-free networks [GPP12]. Due to high clustering coefficients, HRG is more accurate than earlier models such as Preferential Attachment [BA99] in modeling real-world networks.

Perhaps the two most important algorithmic problems related to HRGs are *sampling* (generate a HRG) and *MLE embedding*: given a real-world network $H = (V, E)$, map the vertices of H to the hyperbolic plane in such a way that the edges are predicted as accurately as possible. The quality of this prediction is measured with *log-likelihood*, computed with the formula $\sum_{v,w} \log p(v, w)$, where $p(v, w)$ is the probability that the model correctly predicts the existence or not of edge (v, w) . Those problems are non-trivial: even simply computing the log-likelihood, using a naive algorithm would require time $O(|V|^2)$. The

original paper [PKS⁺12] used an $O(|V|^3)$ algorithm for embedding. Efficient algorithms have been found for generating HRGs in time $O(|V|)$ [BKL18] and for MLE embedding real-world scale-free networks into the hyperbolic plane in time $\tilde{O}(|V|)$ [BFKL16], which was a major improvement over previous algorithms [PAK15, vLMP15]. Embedding has practical applications in link prediction [SJ19] and routing [BPK10, BFKK18].

This paper introduces and experimentally studies the discrete version of the HRG model (DHRG). In the DHRG model, we use a tessellation rather than the hyperbolic plane. Instead of the hyperbolic distance between points, we use the number of steps between two tiles in the tessellation. Our approach has the following advantages:

- Avoiding numerical issues. DHRG is not based on the tuple of coordinates, which makes it immune to serious precision errors resulting from the exponential expansion. This way we solve a fundamental issue for hyperbolic embeddings [BFKK18, SDSGR18].
- Simplicity. In DHRG we find efficient algorithms for sampling, computing the log-likelihood, and improving an embedding by generalizing similar algorithms for trees. Working with DHRG does not require a good understanding of hyperbolic geometry, combating a major drawback of previous approaches.
- Our experiments on artificial networks show that using DHRG improves the success rate of greedy routing in 77% cases (depending on the parameters).
- a DHRG embedding can be efficiently improved by moving the vertices so that the log-likelihood becomes better. Our procedure yields about 10% improvement of log-likelihood on state-of-the-art HRG embeddings on artificial graphs, and up to 24% improvement in the case of real-world graphs.

1 Prerequisites

In this section, we briefly introduce hyperbolic geometry and the HRG model. A more extensive introduction to hyperbolic geometry can be found, e.g., in [CFK⁺97].

Figure 1 shows the order-3 heptagonal tessellation of the hyperbolic plane in the Poincaré model. In the hyperbolic metric, all the triangles, heptagons, and hexagons on each picture are actually of the same size. The points on the boundary of the disk are infinitely far from the center. The area of a hyperbolic circle of radius r is exponential in r .

The hyperbolic plane (in the Minkowski hyperboloid model) is $\mathbb{H}^2 = \{(x, y, z) : z > 0, z^2 - x^2 - y^2 = 1\}$. The distance between two points $a = (x, y, z)$ and

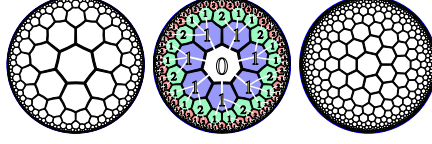


Figure 1: (a) Order-3 heptagonal tiling (G_{710}). (b) Its growth. (c) Bitruncated heptagonal tiling (G_{711}).

$a' = (x', y', z')$ is $\delta(a, a') = \text{acosh}(zz' - xx' - yy')$. Most introductions to hyperbolic geometry use the Poincaré disk model; however, the Minkowski hyperboloid model is very useful in computational hyperbolic geometry, because the essential operations are simple generalizations of their Euclidean or spherical counterparts. In particular, rotation of a point v by angle α is given by

$$\begin{pmatrix} \cos \alpha & \sin \alpha & 0 \\ -\sin \alpha & \cos \alpha & 0 \\ 0 & 0 & 1 \end{pmatrix} v,$$

while a translation by x units along the X axis is given by

$$\begin{pmatrix} \cosh x & 0 & \sinh x \\ 0 & 1 & 0 \\ \sinh x & 0 & \cosh x \end{pmatrix} v.$$

We can easily map the Minkowski hyperboloid model to Poincaré disk model (e.g., for visualization purposes) using stereographic projection:

$$(x', y') = (x/(z+1), y/(z+1)).$$

In the hyperbolic polar coordinate system, every point is represented by two coordinates (r, ϕ) , where

$$P(r, \phi) = (\cos(\phi) \sinh(r), \sin(\phi) \sinh(r), \cosh(r)).$$

Here, r is distance from the central point $(0, 0, 1)$, and ϕ is the angular coordinate.

Definition 1. *The hyperbolic random graph model has four parameters: n (number of vertices), R (radius), T (temperature), and α . Each vertex $v \in V = \{1, \dots, n\}$ is independently randomly assigned a point $\mu(v) = P(r_v, \phi_v)$, where the distribution of ϕ_v is uniform in $[0, 2\pi]$, and the density of the distribution of $r_v \in [0, R]$ is given by $f(r) = \frac{\alpha \sinh(\alpha r)}{\cosh(\alpha R) - 1}$. Then, for each pair of vertices $v, w \in V$, they are independently connected with probability $p(\delta(\mu(v), \mu(w)))$, where $\delta(x, y)$ is the distance between $x, y \in \mathbb{H}^2$, and $p(d) = \frac{1}{1 + e^{(d-R)/2T}}$.*

The parameter α controls the power-law exponent $\beta = 2\alpha + 1$ [GPP12]. The parameter T , typically chosen to be in $[0, 1]$, regulates the importance of

underlying geometry, and thus the clustering coefficient: with T very close to 0, an edge exists iff $\delta(\mu(v), \mu(w)) < R$, while with larger values of T missing short edges and existing long edges are possible. In [BFKL16], $R = 2 \log n + C$, where C is a parameter adjusting the average degree of the resulting graph.

An **MLE embedder** is an algorithm which, given a network $H = (V, E)$, finds a good embedding of H in the hyperbolic plane, i.e., parameters R , T , and α , and a mapping $\mu : V \rightarrow \mathbb{H}^2$. The quality of the embedding is measured with *log-likelihood*, computed with the formula

$$\log L(\mu) = \sum_{v < w \in V} \log p_{\{v, w\} \in E}(\delta(\mu(v), \mu(w))),$$

where $p_\phi(d) = p(d)$ if ϕ is true and $1 - p(d)$ if ϕ is false. Log-likelihood is a measure of the quality of embedding. While not a goal by itself, we can expect that a better embedding (in terms of log-likelihood) will perform better in the applications, such as link prediction, greedy routing, visualization, etc.

Now, we explain the structure of a hyperbolic tessellation, on the example of the order-3 heptagonal tiling (G_{710} from Figure 1b). Distances from the central tile are marked by numbers; we denote this distance for tile t with $\delta_0(t)$. Except for the central tile, every tile has one or two adjacent tiles in the previous layer (called left and right parent, p_L and p_R), two adjacent tiles in the same layer (left and right sibling, s_L and s_R), and the remaining tiles in the next layer (children). By connecting every tile to its (right) parent, we obtain an infinite tree structure. The numbers 0, 1, 2 denote the *type* of the tile, which is the number of parents. We represent this structure as a lazily generated tree of pointers (the types of all tiles are determined uniquely by the parent's type and the child's index). Non-tree adjacencies can also be found and represented in our structure in amortized time $O(1)$. Since every tile has at least two (non-rightmost) children, this structure grows exponentially. To gain intuition about hyperbolic tessellations, we recommend playing HyperRogue [KCv17] as its gameplay focuses on the crucial concepts of exponential growth and distances in the tessellation graph.

While Euclidean tessellations can be scaled arbitrarily, this is not the case for hyperbolic tessellations. The distance x between the centers of two adjacent tiles is the edge length of a triangle with angles $\pi/7$, $\pi/7$, and $2\pi/3$, which we can find using the hyperbolic cosine rule. If the central tile is at Minkowski hyperboloid coordinates $(0, 0, 1)$, the coordinates of every other tile t can be found using translations (by x units) and rotations (by multiples of $2\pi/7$).

2 Our contribution

Here we introduce the hyperbolic random graph model (DHRG), which is the discrete version of the HRG model (Definition 1). We map vertices $v \in V$ not to points in the continuous hyperbolic plane but the tiles of our tessellation, i.e., $\mu : V \rightarrow D_r$, where D_r is the set of all tiles in distance at most R .

Definition 2. A discrete hyperbolic random graph (DHRG) with parameters n , R , T , and α is a random graph $H = (V, E)$ constructed as follows:

- The set of vertices is $V = \{1, \dots, n\}$,
- Every vertex $v \in V$ is independently randomly assigned a tile $\mu(v) \in D_r$, in such a way that the probability that $\mu(v) = w$ is proportional to $\frac{e^{d\alpha}}{|R_d(G)|}$, where $d = \delta_0(w)$, and $R_d(G)$ is the set of tiles in distance d ;
- Every pair of vertices $v_1, v_2 \in V$ are independently connected with an edge with probability $p(\delta(\mu(v_1), \mu(v_2)))$, where $p(d) = \frac{1}{1+e^{(d-R)/2T}}$.

Note that the definition permits $\mu(v_1) = \mu(v_2)$ for two different vertices $v_1, v_2 \in V$ – this is not a problem; such vertices v_1 and v_2 are not necessarily connected, nor do they need to have equal sets of neighbors. This may happen when two vertices are too similar to be differentiated by our model.

Determining the relation between discrete and continuous distances theoretically is challenging. We find this relation experimentally. We compute the hyperbolic distance R_d between $h_0 = (0, 0, 1)$ and T_d , where T_d is a randomly chosen tile such that $\delta_0(T_d) = d$. We get $R_d = 0.9696687d + 1.05603207 + X_d$, where $EX_d = o(1)$, $\text{Var } X_d = \Theta(d)$, and X_d has a bell-shaped distribution. Table 1 contains the example detailed results for G_{710} .) The asymptotic val-

d	n_d	ER	$\text{Var}(R)$
0	1	0.00000000	0.00000000
1	7	1.09054966	0.00000000
2	21	2.02973974	0.02467308
3	56	2.99594181	0.03923368
4	147	3.96512066	0.05370197
5	385	4.93471877	0.06823850
6	1008	5.90437726	0.08279668
7	2639	6.87404448	0.09735968
8	6909	7.84371297	0.11192362
9	18088	8.81338165	0.12648772
10	47355	9.78305035	0.14105185
11	123977	10.75271905	0.15561599
12	324576	11.72238775	0.17018013
13	849751	12.69205646	0.18474427
14	2224677	13.66172516	0.19930841
15	5824280	14.63139386	0.21387255
16	15248163	15.60106257	0.22843669

Table 1: Tessellation distances (d) versus hyperbolic distances (R_d): expected value and variance.

ues are obtained in the following way: the difference $R_d - R_{d-1}$ converges very

quickly to 0.9696687, and the difference $R_d - 0.9696687d$ converges very quickly to 1.05603207. Note that the error is much better than for Euclidean hex grid, where a similar formula holds, but with $\text{Var } X_d = \Theta(d^2)$. This is because in the Euclidean plane, the stretch factor depends on the angle between the line $[h_0, T_d]$ and the grid, which remains constant along the whole line; on the other hand, in the hyperbolic plane, this angle is not constant, and its values in sufficiently distant fragments of that line are almost independent. The number n_d in Table 1 is the number of tiles in distance d ; they are every second Fibonacci number multiplied by 7, and thus $n_d = \Theta(\gamma^d)$ for $\gamma = 2.618\dots$. The radius of a hyperbolic disk which has the same area as the union of all tiles in distance at most d is $\log(\gamma)d + O(1)$; our coefficient $c_1 = 0.9696687$ is close to $\log(\gamma) = 0.962424$, but slightly larger.

Let j be a function which maps every tile of our tessellation to its center. DHRG mappings can be converted to HRG by composing μ with j , and the other conversion can be done by finding the tile containing $\mu(v)$ for each $v \in V$. Based on our experimental evaluation, we expect the DHRG model to have similar properties to the HRG model, because distances in hyperbolic tessellations have similar properties to continuous hyperbolic distances. The parameters α , R and T of the DHRG model will be obtained from the HRG parameters by dividing them by c_1 .

3 Algorithms for DHRG

In this section, we present our algorithms for working efficiently with the DHRG model.

Proposition 1. *There is a canonical shortest path between every pair of tiles (t_1, t_2) . If t_2 is to the right from t_1 , this canonical shortest path consists of: a number of right parent edges; at most one right sibling edge; and a number of non-leftmost child edges. If t_1 is to the right from t_2 , the canonical path is defined symmetrically. For any pair of tiles (t_1, t_2) , the distance $\delta(t_1, t_2)$ can be found in time $O(\delta(t_1, t_2))$.*

The algorithm for finding $\delta(t_1, t_2)$ works as follows: for every d from $\min(\delta_0(t_1), \delta_0(t_2))$, we find $p_L^{\delta_0(t_1)-d}(t_1)$, $p_R^{\delta_0(t_1)-d}(t_1)$, $p_L^{\delta_0(t_1)-d}(t_2)$, and $p_L^{\delta_0(t_1)-d}(t_2)$. If one of the tiles from t_1 matches one of the tiles from t_2 , we return $\delta_0(t_1) + \delta_0(t_2) - 2d$; if they don't match but are adjacent, we return $\delta_0(t_1) + \delta_0(t_2) - 2d + 1$.

In our application, we will need to efficiently find the distance between a tile t and all tiles $u \in A$. We will do it using the following data structure:

Definition 3. *A distance tally counter is a structure with the following operations:*

- INIT, which initializes the multiset A to empty.
- ADD(u, x), which adds u to the multiset A with multiplicity x (which can be negative).

- $\text{COUNT}(t)$, which returns an array T such that $T[d]$ is the number of elements of A in distance d from t .

Theorem 1. *There is an implementation of distance tally counter where all the operations are executed in $O(R^2)$, where R is the maximum distance from the central tile.*

Proof. A **segment** is a pair of tiles of form $[p_L^k(t), p_R^k(t)]$ for some tile t and $k \geq 0$. For a segment $s = [v_L, v_R]$, let $p(s) = [p_L(v_L), p_R(v_R)]$ be the parent segment. In the case of the order-3 heptagonal tessellation, either $p_L^k(t) = p_R^k(t)$, or they are neighbors. The algorithm from Proposition 1 can be seen as follows: we start with two segments $[t_1, t_1]$ and $[t_2, t_2]$, and then apply the parent segment operation to each of them until we obtain good segments which are close. To construct an efficient distance tally counter, we need to tally the ancestor segments for every $u \in A$.

For every segment s , we keep an array a_s , where $a_s[d]$ is the number of $u \in A$ such that $p^d[u, u] = s$. The operation ADD updates these arrays in time $O(R^2)$. The operation $\text{COUNT}(t)$ constructs $s_d = p^d[t, t]$ for $d = 0, \dots, \delta_0(t)$, and uses the information in segments intersecting or adjacent to s_d to count the number of elements of u for which the distance algorithm would return every possible distance. We need to make sure that we don't count the same $u \in A$ twice (for different values of d); however, this can be done by temporarily subtracting from $a_s[d]$ entries which correspond to u 's which have been already counted. \square

Other tessellations than the order 3 heptagonal tessellation are possible, such as G_{711} from Figure 1. Finer tessellations can be obtained by applying the Goldberg-Coxeter construction; their exponential growth is less extreme than for G_{710} , and thus not everything above holds without changes (the distance of segment ends, as well as the number of sibling edges in the canonical path, may be greater than 1; but they are still bounded). Let $D(G)$ be the bound; for tessellations useful in practice the value of $D(G)$ is small, we have $D(G_{710}) = 1$ and $D(G_{711}) = 3$. Coarser tessellations can be obtained by using octagons rather than heptagons.

Generalization of Proposition 1. For $D(G) > 1$, there is one more type of a canonical path possible, where w is a parent of v , but neither the leftmost nor rightmost one.

The idea of the algorithm is to find the shortest canonical path. Suppose that $\delta_0(v) = d' + \delta_0(w)$, where $d' \geq 0$. For each i starting from 0 we compute the endpoints of the segments $P^{d'+i}(v)$ and $P^i(w)$. We check whether these segments are in distance at most γ on the ring; if no, then we can surely tell that we need to check the next i ; if yes, we know that the shortest path can be found on one of the levels from i to $i + \lfloor \gamma/2 \rfloor$. We compute the length of all such paths and return the minimum.

The pseudocode of our algorithm is given below. It uses five integer variables a_i, d_i, d and four tile variables l_i, r_i ($i = 1, 2$). Variables a_i, d_i, l_i and r_i are modified only by the function $\text{push}(i)$, which lets us keep the following invariant:

$\delta_0(l_i) = \delta_0(r_i) = d_i$, $l_i = p_L^{a_i}(v_i)$, $r_i = p_R^{a_i}(v_i)$. By $v + k$, where v is a tile, we denote the k -th right sibling of v .

The lines (16-17) deal with the special case for $D(G) > 1$ mentioned above.

The main loop in lines (19-23) deals with the other cases. At all times d is the currently found upper bound on $\delta(v, w)$. It is easy to check that the specific shortest path given in Proposition 1 will be found by our algorithm.

Every iteration of every loop increases a_1 or a_2 , and an iteration can occur only if $a_1 + a_2 < \delta(v, w)$. Therefore, the algorithm runs in time $O(\delta(v, w))$.

```

1. function DISTANCE( $v_1, v_2$ ):
2.   for  $i \in \{1, 2\}$ :
3.      $l_i := v_i$ 
4.      $r_i := v_i$ 
5.      $d_i := \delta_0(v_i)$ 
6.      $a_i := 0$ 
7.   function push( $i$ ):
8.      $a_i := a_i + 1$ 
9.      $d_i := d_i - 1$ 
10.     $l_i := p_L(l_i)$ 
11.     $r_i := p_R(r_i)$ 
12.  while  $d_1 > d_2$  :
13.    push(1)
14.  while  $d_2 > d_1$  :
15.    push(2)
16.  for  $i \in \{1, 2\}$  if  $v_i \in [l_i, r_i]$  :
17.    return  $a_{3-i}$ 
18.   $d := \infty$ 
19.  while  $a_1 + a_2 < d$ :
20.    for  $i \in \{1, 2\}$  for  $k \in \{0, \dots, D(G)\}$  if  $l_i = r_{3-i} + k$  :
21.       $d := \min(d, a_1 + a_2 + k)$ 
22.    push(1)
23.    push(2)
24.  return  $d$ 

```

□

Proof of Theorem 1 for the general case. A segment is **good** if it is of the form $P^d([v, v])$ for some $v \in V$ and $d \in \mathbb{N}$. In our algorithm the operation $\text{ADD}(w)$ will update the information in the good segments of the form $P^d([w, w])$, and the operation $\text{COUNT}(v)$ will follow the algorithm from Proposition 1, but instead of considering the single segment $[w, w]$, it will count all of them, by using the information stored in the segments close to $P^d([v, v])$. Our algorithm will optimize by representing all the good segments coming from tiles v added to our structure.

We call a tile or good segment *active* if it has been already generated, and thus is represented as an object in memory. For each active tile $v \in V$ we keep two lists $L_L(v), L_R(v)$ of active segments S such that v is respectively the leftmost and rightmost element of S . Each active segment S also has a pointer to $P(S)$, which is also active (and thus, all the ancestors of S are active too), and a dynamic array of integers $a(S)$. Initially, there are no active tiles or good segments; when we activate a segment S , its $a(S)$ is initially filled with zeros. The value of $a(S)[i]$ represents the total $f(w)$ for all tiles w which yield the segment S after i operations of the algorithm from the proof of Proposition 1, i.e., $a(S)[i] = \sum_{w: P^i([w, w]) = S} f(w)$.

The operation $\text{ADD}(w, k)$ works as follows: for each $i = 0, \dots, \delta_0(v)$, we simply add k to $a(P^i(S))[i]$. In the pseudocode below, we assume that $P(S)$ returns **null** if S is the root segment.

1. **function** $\text{ADD}(w, x)$:
2. $S := [w, w]$
3. $i := 0$
4. **while** $S \neq \text{null}$:
5. $a(S)[i] = a(S)[i] + x$
6. $S := P(S)$
7. $i := i + 1$

The operation $\text{COUNT}(v)$ activates v and $S = [v, v]$ together with all its ancestors. We return the vector A obtained as follows. We look at $P^i(S)$ for $i = 0, \dots, \delta_0(v)$, and for each $P^i(S)$, we look at close good segments q' on the same level, lists $L_L(w), L_R(w)$ for all w in distance at most γ from $P_i(S)$. The intuition here is as follows: the algorithm from Proposition 1, on reaching $p^{i_1}(v) = S$ and $p^{i_2}(w) = S'$, would find out that these two pairs are close enough and return $i_1 + i_2 + \delta(S, S')$; in our case, for each c such that $a(S')[c] \neq 0$, we will instead add $a(S')[c]$ to $A[a_1 + \delta(S, S') + c]$.

We have to be careful that, if we count some vertex v when considering the pair of segments (S, S') , we do not count it again when considering the pair of segments $(P^j(S), P^j(S'))$. This is done in lines 18–21 in the pseudocode below. By S^L and S^R we respectively denote the leftmost and rightmost vertex of the segment S .

1. **function** $\text{COUNT}(v)$:

```

2.    $U = \emptyset$ 
3.   for each active  $S' \ni v$ :
4.        $\text{insert}(U, (S', 0))$ 
5.    $d := 0$ 
6.    $S := [v, v]$ 
7.   while  $S \neq \text{null}$  :
8.       for  $i \in 0, \dots, D(G)$  :
9.           for each  $S' \in L_R(S^R + i)$ :
10.               $\text{insert}(U, (S', d + \delta(S, S')))$ 
11.           for each  $S' \in L_L(S^L - i)$ :
12.               $\text{insert}(U, (S', d + \delta(S, S')))$ 
13.        $d := d + 1$ 
14.        $S := P(S)$ 
15.    $T = []$ 
16.   for each  $(S', d) \in U$ :
17.       for each  $i$ :  $T[d + i] = T[d + i] + a(S')[i]$ 
18.        $S'' := P(S')$ 
19.       if  $(S'', d') \in U$  for some  $d'$ :
20.           for each  $i$ :  $T[d' + i] = T[d' + i] - a(S')[i]$ 
21.           break
22.   return  $T$ 

```

□

Computing the likelihood. Computing the log-likelihood in the continuous model is difficult, because we need to compute the sum over $O(n^2)$ pairs; a better algorithm was crucial for efficient embedding of large real-world scale-free networks [BFKL16]. The algorithms above allow us to compute it quite easily and efficiently in the DHRG model. To compute the log-likelihood of our embedding of a network H with n vertices and m edges, such that $\delta_0(v) \leq R$ for each $v \in V$, we:

- for each d , compute $\text{PAIRS}[d]$, which is the number of pairs (v, w) such that $\delta(v, w) = d$ – the distance tally counter allows doing this in a straightforward way (simply by doing $\text{Add}(\mu(v))$ for each $v \in V$), in time $O(nR^2)$.
- for each d , compute $\text{EDGES}[d]$, which is the number of pairs (v, w) connected by an edge such that $\delta(v, w) = d$ – this can be done in time $O(mR)$ simply by using the distance algorithm for each of m edges.

grid	L_4	L_6	L_3	L_5	L_2	L_7	MB	#it	time
G_{810}	-186163	-170175	-187738	-172018	-176131	-172585	46	37	19 s
G_{710}	-181134	-168006	-182721	-170074	-176131	-170873	40	29	17 s
G_{711}	-177033	-165338	-179125	-167991	-176131	-168445	61	23	23 s
G_{720}	-178054	-165671	-179977	-168105	-176131	-168817	98	71	97 s
G_{721}	-175826	-164643	-178108	-167407	-176131	-167824	146	99*	288 s
G_{753}	-175048	-164003	-177254	-166889	-176131	-167648	1050	99*	5004 s
B_2	-178494	-165792	-180354	-168055	-176131	-168338	47	15	24 s
$B_{1.1}$	-177921	-166561	-180112	-169019	-176131	-168134	54	11	11 s
$B_{1.0}$	-177505	-166374	-179554	-168717	-176131	-168214	53	59	16 s
$B_{0.9}$	-177388	-166487	-179500	-168973	-176131	-168282	56	45	30 s
$B_{0.5}$	-177657	-166482	-179742	-168906	-176131	-168017	62	7	14 s
$\{5, 4\}$	-194905	-171835	-195952	-173641	-176131	-175671	38	20	10 s

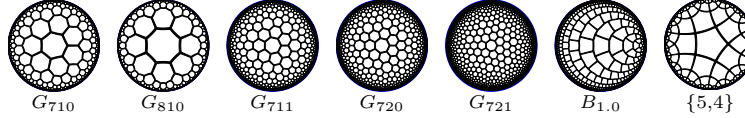


Table 2: Experimental results on the Facebook network.

After computing these two values for each d , computing the log-likelihood is straightforward. One of the advantages over [BFKL16] is that we can then easily compute the log-likelihood obtained from other values of R and T , or from a function $p(d)$ which is not necessarily logistic.

Improving the embedding. A continuous embedding can be improved by a *spring embedder* [KW04]. Imagine there are attractive forces between connected pairs of vertices, and repulsive forces between unconnected pairs. The embedding m changes in time as the forces push the vertices towards locations in such a way that the quality of the embedding is improved. Computationally, spring embedders are very expensive – there are $O(n^2)$ forces, and potentially many steps of simulation could be necessary.

On the contrary, our approach allows to improve DHRG embeddings easily. We use a local search algorithm. Suppose, we have computed the log-likelihood and on the way we have computed the vectors PAIRS and EDGES, as well as the distance tally counter where every $\mu(v)$ has been added. Let $v' \in V$ be a vertex of our embedding, and w be a tile. Let μ' be the new embedding given by $\mu'(v') = w$ and $\mu'(v) = \mu(v)$ for $v \neq v'$. Our auxiliary data lets us compute the log-likelihood of μ' in time $O(R^2 + R \deg(w))$.

We try to improve the embedding in the following way: in each iteration, for each vertex $v \in V$, consider all neighbors of $\mu(v)$, compute the log-likelihood for all of them, and if for some μ' we have $\log L(\mu') > \log L(\mu)$, replace μ with μ' . Each iteration takes time $O(R^2 n + Rm)$.

4 Experiments on real-world networks

All the times are measured on Intel(R) Core(TM) i7-9700K CPU @ 3.60GHz. Most computations use a single core, except the continuous loglikelihood values (L_2 and L_7) which use 8 cores. Our implementation, using the RogueViz non-Euclidean geometry engine [KCK21], as well as the results of our experiments can be found at https://figshare.com/articles/software/Discrete_Hyperbolic_Random_Graph_Model_code_and_data_/16624369.

Small real-world network. First, we test our model on a medium size network ($n = 4039$ nodes and $m = 88234$ edges). We have chosen the Facebook social circle network from the SNAP database [LK14] and provided with the hyperbolic embedder implementing the algorithm from [BFKL16] (BFKL). BFKL mapped this graph to the hyperbolic plane using parameters $R = 12.576$, $\alpha = 0.755$, $T = 0.1$. The log-likelihood is $L_1 = -516534$; it is worse than the log-likelihood of the naive model where each edge exists with probability $m/\binom{n}{2}$ ($L_0 = -487133$). This is because the influence of the parameter T on the quality of the embedding is small [PAK15]; BFKL uses a small value of $T = 0.1$ that does not necessarily correspond to the network. The best log-likelihood of $L_2 = -176131$ is obtained for $R_2 = 11.09358$ and $T_2 = 0.54336$.

We convert this embedding into the DHRG model, by finding the nearest tile of G_{710} for each $v \in V$. The best log-likelihood $L_3 = -182721$ is obtained for $R_3 = 11.41784$ and $T_3 = 0.58948$; as predicted in Section 2, $T_2/T_3 \approx R_2/R_3 \approx \log \gamma$. Our log-likelihood L_3 is slightly worse than L_2 , but this is not surprising. First, our edge predictor has lost some precision in the input because of our tessellation’s discrete nature. Second, the original prediction was based on the hyperbolic distance r while our prediction is based on the tessellation distance d , and the ratio of r and d depends on the direction. We also compute the log-likelihood obtained by a model where the edge probability is $p(d) = \text{EDGES}[d]/\text{PAIRS}[d]$, which corresponds to using the best possible function $p(d)$ (not necessarily logistic); we obtain $L_4 = -188134$, which is only slightly better than L_3 .

Next, we try our local search algorithm. The points stopped moving in the 29th iteration. This improved the log-likelihood to $L_5 = -170074$, again for the best values of $R_5 = 11.50793$ and $T_5 = 0.55546$, and the optimal log-likelihood to $L_6 = -168006$.

Now, we convert our mapping back to the HRG model, obtaining the log-likelihood of $L_7 = -170889$ for the optimal values of $R_7 = 10.96077$ and $T_7 = 0.53555$. Note that L_7 is significantly better than L_2 ; hence, despite converting from HRG to DHRG and back, we found a better embedding.

The running time of parts of our algorithm were: $t_1=0.3$ s (converting), $t_2=0.016$ s (computing EDGES), $t_3=0.16$ s (computing PAIRS), $t_4=12$ s (local search). The BFKL embedder computes the log-likelihood in 0.2 seconds, which is comparable. However, their spring embedder working in quadratic time is much slower than our local search.¹

¹For $T = 0.54336$ and seed 123456789 the BFKL spring embedder reported the log-likelihood of -131634, which is better than ours; however, our implementation reports

name	n	R	α	grid	L_4	L_6	L_3	L_5	MB	#it	t [s]
Facebook	4309	12.57	0.755	G_{710}	-181134	-168002	-182721	-170078	40	20*	10
Facebook	4309	12.57	0.755	G_{810}	-186163	-170176	-187738	-172026	54	20*	8
Followers09	74946	20.90	0.855	G_{710}	-4021755	-3522077	-4122113	-3538064	2010	20*	222
Followers09	74946	20.90	0.855	G_{810}	-4088809	-3520177	-4178102	-3529118	1866	20*	176
Slashdot	77352	26.00	0.610	G_{710}	-2573745	-1866407	-2611129	-1879685	2659	20*	201
Slashdot	77352	26.00	0.610	G_{810}	-2639252	-1875482	-2663357	-1890126	2253	20*	158
Amazon	334863	24.11	0.995	G_{710}	-6911106	-6075602	-7220125	-6189928	5677	20*	721
Amazon	334863	24.11	0.995	G_{810}	-6986382	-6087990	-7265464	-6183186	4868	20*	576
Followers11	405270	26.34	0.715	G_{710}	-24127217	-18392232	-24350405	-18461108	9995	20*	1349
Followers11	405270	26.34	0.715	G_{810}	-24275831	-18379753	-24405855	-18433429	8940	20*	1113
Google	855804	26.06	0.865	G_{710}	-29173754	-22168269	-29626431	-22264111	18226	20*	2363
Google	855804	26.06	0.865	G_{810}	-29628588	-22292392	-30034845	-22383101	15314	20*	1823
Patents	3764118	28.74	0.995	G_{810}	-206451894	-188056879	-208618134	-188589723	66396	20*	9335

Table 3: Experimental results on real-world networks. Facebook, Slashdot, Amazon, Google, and Patents networks from SNAP database.

name	grid	L_2	L_7	t [s]
Facebook	G_{710}	-176131	-170889	0.35
Facebook	G_{810}	-176131	-172573	0.5
Followers09	G_{710}	-3954627	-3550804	131
Followers09	G_{810}	-3954627	-3556817	128
Followers11	G_{710}	-20028756	-18650426	3715
Followers11	G_{810}	-20028756	-18654664	3636
Slashdot	G_{710}	-2091651	-1916378	130
Slashdot	G_{810}	-2091651	-1929044	126
Amazon	G_{710}	-6957174	-6305189	2690
Amazon	G_{810}	-6957174	-6283523	2811
Google	G_{710}	-22762281	-22294348	16618
Google	G_{810}	-22762281	-22432501	15818

Table 4: Improvements in the continuous loglikelihood.

Large real-world networks. To benchmark our algorithm on a large network, we study the embedding of a social network with power-law-like scale behavior (undirected graph; $n=74946$ nodes and $m=537952$ edges), representing the following relations that occurred in 2009 in GitHub [Cel16] (see the Technical Appendix for the details). In GitHub convention, *following* means a registered user agreed to be sent notifications about other user’s activity within the service. We represent this relationship using the following graph \mathcal{G}_f . There is an edge in \mathcal{G}_f between A and B if and only if A follows B. Mechanisms behind the creation of this network involve users’ popularity and the similarity, which suggests underlying hyperbolic geometry of \mathcal{G}_f . \mathcal{G}_f also shows power-law-like scale behavior [Cel16]; we believe it is a useful benchmark for our analysis. Since the complete download of GitHub data is impossible, our dataset is combined from two sources: GHTorrent project [Gou13] and GitHubArchive project [Gri12]. The analyzed network contains information about the following relationships that occurred in the service from 2008 to 2009.

The BFKL embedder has chosen parameters $R = 20.9037$ and $\alpha = 0.855$ and computes the log-likelihood in 5 s. The results for G_{710} are: $t_1 = 6$ s, $t_2 = 1.5$ s, $t_3 = 0.5$ s, $L_0 = -4364526$, $L_2 = -3954627$, $L_3 = -3976515$, $T_3 = 1.398666$, $R_3 = 9.063012$, $L_4 = -3859688$. After 6 iterations of local search (25s each) the results have been improved to $L_5 = -3571941$, $L_6 = -3542740$; after 100 iterations the results are only slightly better, at -3545664 and -3527397 , $L_7 = -3550804$. The time $t_2 + t_3$ is still comparable to BFKL. On a larger follower network (years 2008-2011, 405270 vertices) our local search improves the log-likelihood by about 24%.

Table 3 presents the experimental results of running our algorithm on other larger graphs. The parameters n , R and α come from the BFKL embedder (n is the number of vertices). The rest of values are as in the previous table. As we can see, on most of the larger graphs, our algorithm improves the log-likelihoods by about 25%. The current version uses a significant amount of RAM. It should be possible to improve this by better memory management (currently vertices and segments which are no longer used or just temporarily created are not freed), or possibly path compression. Table 4 shows the value of L_2 and L_7 for every graph (computing L_2 and L_7 is not feasible for the Patents database), as well as the time of computing these values.

Choice of the tessellation. Other tessellations than G_{710} are also possible. Finer tessellations give better log-likelihoods, but a too dense grid dramatically decreases the performance without giving significant benefits.

Table 2 presents the experimental results of running our algorithm on the Facebook social circle network graph for various tessellations. We can obtain a coarser grid than G_{710} by using octagons instead of heptagons (G_{810}), and a finer

$L_1 = -211454$ and $L_2 = -174465$, which our local search still manages to improve to $L_7 = -170889$. This appears to be a problem in their approximation (which also affects the fast embedder and smaller values of T). Indeed, replacing their optimized log-likelihood function with a $\Theta(n^2)$ one from `hyperbolic.cpp` yields result equal to ours. [Actually, it reports double our result, but this seems to be caused by counting each pair of vertices twice, which is easy to fix and irrelevant for the optimized embedder.]

grid by using the Goldberg-Coxeter construction, which adds extra hexagons to the order-3 heptagonal tessellation (G_{7ab}). We can also use a tessellation B_x based on the binary tiling [Bö74] (where x is the width of the tile), or $\{5, 4\}$, where four pentagons meet in a vertex. Log-likelihoods are named as in Section 4:

L_2, L_7 – continuous log-likelihood with optimal R, T

L_3, L_5 – discrete log-likelihood, logistic function with optimal R, T

L_4, L_6 – discrete log-likelihood, arbitrary function of distance (used for local search)

The column #it presents the number of iterations of local search; * denotes that we have stopped the process after this number of iterations, while no * denotes that the local search could not improve the log-likelihood any further. MB is the amount of memory in megabytes, and time is in seconds.

As we can see, finer tessellations give better log-likelihoods, but a too dense grid dramatically decreases the performance without giving significant benefits. Tessellation B_x does not yield significantly better results, despite its circles’ greater similarity to continuous ones. The results of $\{5, 4\}$ are relatively bad; it approximates distances worse than three-valent tessellations.

5 Experiments on simulated graphs

5.1 Log-likelihood

In the experiment on the Facebook graph, we have computed the log-likelihood of the BFKL embedding with optimal parameters (L_2), converted it to the DRHG model, optimized it, converted back to the HRG model, and found that the new log-likelihood with optimal parameters (L_7) is better than L_2 . For larger real-world networks the improvement was even better. This section generalizes those results by conducting simulations.

We use the generator included with [BFKL16] to generate HRGs with the following parameters: varying n , $\alpha = 0.75$, $T = 0.1$, $R = 2 \log(n) - 1$. These are the default values of parameters used by this generator. For every value of n considered, we have generated 1000 graphs. For each of the generated graphs, we have embedded G using BFKL, computed L_2 , converted to DHRG, improved the embedding (up to 20 iterations), converted back to HRG, and computed L_7 . We have also computed L_g , which is the log-likelihood of the originally generated embedding (groundtruth).

Figure 2 shows the density graph of L_2/L_g and L_7/L_g for every n . Since L_g is negative, larger values of these ratios are worse. We know that an optimal embedder should achieve log-likelihood at least as good as L_g . We find that our algorithm yields a significant improvement.

According to the data in Table 5, we notice that our procedure leads to better embeddings than the pure BFKL embedder no matter the size of the graph. Our procedure yields log-likelihoods that are closer to the log-likelihood of the groundtruth. The improvement towards groundtruth is not stable; with the

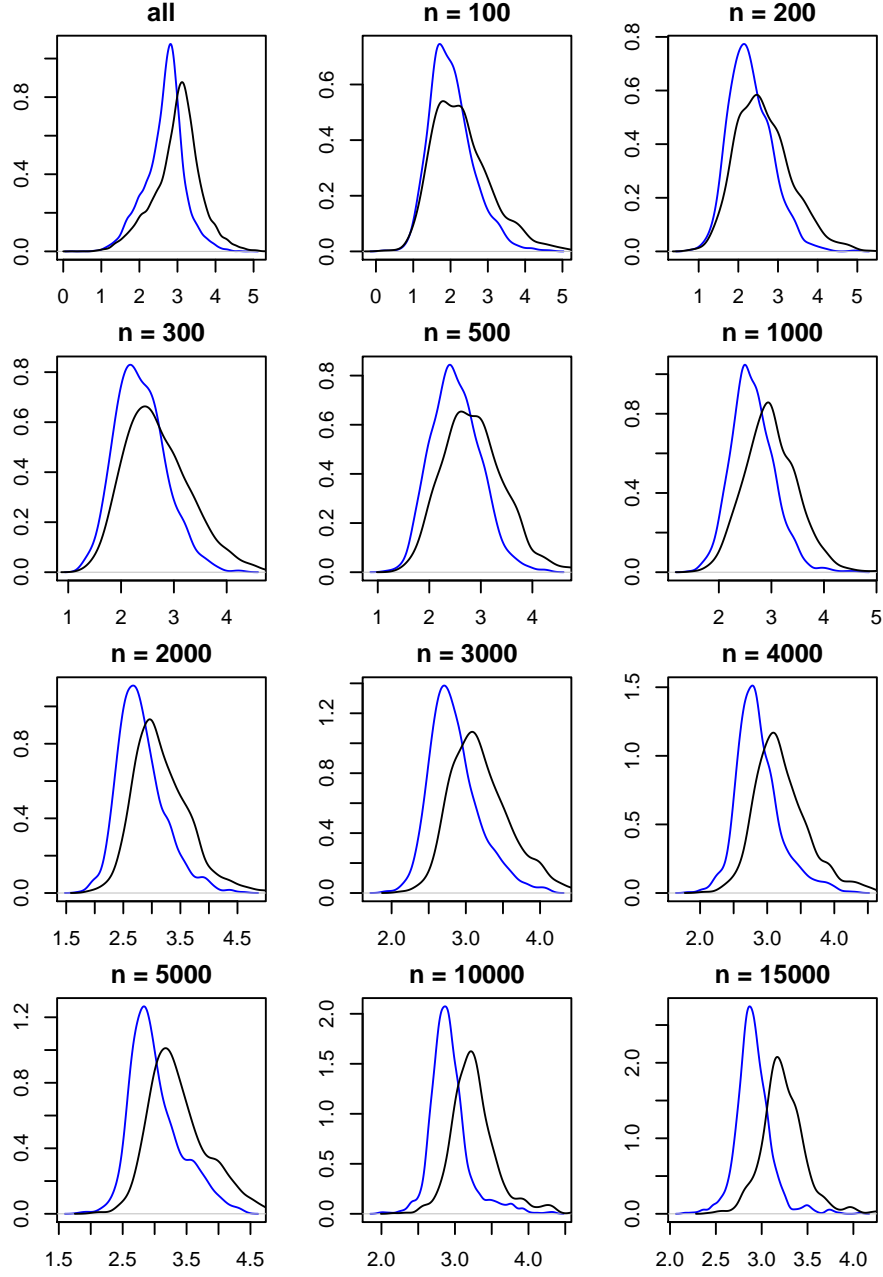


Figure 2: Density of L_2/L_g (black) and L_7/L_g (blue) for $T = 0.1$.

n	improved	rel. to 0		groundtruth	
		avg	median	avg	median
100	84.6	12.8	11.9	36.2	22.0
200	95.2	12.5	12.1	20.6	20.4
300	97.2	11.8	10.6	18.6	17.5
500	99.1	11.5	11.1	18.0	17.5
1000	99.6	11.4	11.0	17.2	16.8
2000	100.0	11.0	10.7	16.2	15.9
3000	100.0	10.9	10.7	15.9	15.8
4000	100.0	10.6	10.4	15.4	15.2
5000	100.0	10.5	10.3	15.0	14.7
10000	100.0	10.3	10.2	14.8	14.7
15000	100.0	10.0	9.9	14.5	14.4

Table 5: Changes in log-likelihood after applying our procedure to BFKL embedders. Percent of improvements signifies the percent of cases the log-likelihood increased (improved). Average and median improvements computed conditionally on improvement. In the "rel. to 0" columns, we present the values of $100 \cdot (1 - L_7/L_2)$; in the "groundtruth" column, we present the values of $100 \cdot (1 - (L_g - L_7)/(L_g - L_2))$.

increase of the graph the BFKL embeddings converge, so our improvements become less prominent (around 15% for large graphs). However, the improvements are statistically significant (p-value for paired Wilcoxon test with alternative hypothesis that the values of log-likelihood increased after our procedure always 0.00).

In real-life cases, hardly do we know the groundtruth; comparison of log-likelihoods for BFKL embedder and our procedure resembles what would we do with real data (columns rel. to zero in Table 5). In such a case, we may expect that our procedure should improve the result by average by 10%. This result seems stable no matter the size of the graph.

5.2 Greedy routing

One potential application of hyperbolic embedding is greedy routing [BPK10, BFKK18]. A node v obtains a packet to node w ; if w is not directly connected to v , v needs to select one of its neighbors through which the packet will be forwarded. In the greedy routing approach, we use the embedding to select the connected node which is the closest to the goal w . Greedy routing fails if, at some point in the chain, none of the connected nodes is closer to w than v itself. In [BPK10] a hyperbolic embedding of the Internet is constructed, yielding 97% success rate of greedy routing. This is much better than a similar algorithm based on geographical placement of nodes (14%). High success rate is also

n	deterioration (discretization)			improvement (local search)			improvement (three steps)			
	%	med	avg	%	med	avg	%	med	avg	p-value
100	95.3	3.28	5.14	81.1	2.55	3.71	56.4	1.11	1.81	0.001
200	97.3	3.27	4.70	82.5	2.24	3.10	53.8	0.99	1.35	0.037
300	99.0	3.25	4.37	85.7	1.97	2.51	55.3	0.91	1.21	0.000
500	99.7	3.19	4.34	87.9	1.81	2.38	55.7	0.71	1.00	0.005
1000	100.0	3.25	3.92	90.8	1.66	1.99	54.0	0.51	0.70	0.071
2000	100.0	3.27	3.73	94.3	1.58	1.73	51.6	0.40	0.50	0.806
3000	100.0	3.27	3.61	98.6	1.53	1.68	49.7	0.33	0.40	0.999
4000	100.0	3.33	3.52	98.6	1.55	1.63	49.0	0.29	0.37	0.999
5000	100.0	3.31	3.52	98.4	1.52	1.61	46.9	0.27	0.36	0.999
10000	100.0	3.27	3.37	99.8	1.56	1.60	42.1	0.19	0.23	1.000
15000	100.0	3.37	3.39	99.9	1.61	1.62	32.2	0.16	0.19	1.000

Table 6: Changes in the success rate of greedy routing (tessellation G_{710}). Average and median computed conditionally on change. P-values for Wilcoxon paired tests.

very robust when we remove some nodes. While the MLE method of finding embedding yields worse results than embeddings constructed specifically for the purpose of greedy routing [BFKK18], it is interesting to see how good our methods are according to this metric.

For the graphs from Section 5.1, we perform three steps:

discretization we convert the embedding to DHRG.

local search we improve the log-likelihood of our embedding using our local search method.

de-discretization we convert the embedding back to HRG.

Table 6 summarizes the changes in success rates after our procedure. We discuss the conditional changes (improvement on the condition of the improvement or deterioration on the condition of the deterioration), because we find the absolute changes possibly misleading for small networks. Percent of changes proxies us the probability of the effect. If the effect occurs, we know what to expect without the bias of the counter-effect. The success rates of the original embedding are around 93% on average. Discretization usually worsens the success probability. This appears to be caused by the fact that two neighbors of v can be in the same distance to w (because of discretization), while originally the more useful node is closer. We notice that if the deterioration due to discretization occurs, the average percentage deterioration decreases with the increasing size of the graph. This is expected, since the distances are larger in larger graphs. Meantime, the median deterioration (if the deterioration occurs) is stable at around 3%. This means that with the increasing size of the network we face serious deteriorations after discretization less often. The effect is statistically significant (p-values of

n	deterioration (discretization)			improvement (local search)			improvement (three steps)			
	%	med	avg	%	med	avg	%	med	avg	p-value
100	86.4	1.65	2.76	72.5	1.67	2.59	61.0	1.00	1.68	0.00
200	90.8	1.67	2.49	78.9	1.61	2.25	63.1	0.94	1.42	0.00
300	94.5	1.59	2.30	82.0	1.42	1.97	65.9	0.84	1.19	0.00
500	98.2	1.57	2.16	86.8	1.35	1.69	67.6	0.80	1.04	0.00
1000	99.4	1.65	1.96	93.9	1.23	1.42	70.4	0.59	0.73	0.00
2000	99.8	1.61	1.82	94.3	1.16	1.27	72.6	0.48	0.60	0.00
3000	99.8	1.64	1.75	96.4	1.15	1.21	74.2	0.42	0.49	0.00
4000	100.0	1.65	1.76	98.1	1.11	1.19	74.0	0.40	0.45	0.00
5000	100.0	1.63	1.75	98.3	1.15	1.20	78.2	0.40	0.46	0.00
10000	100.0	1.61	1.67	99.6	1.17	1.19	82.5	0.36	0.38	0.00
15000	100.0	1.64	1.66	99.7	1.19	1.20	87.0	0.32	0.33	0.00

Table 7: Changes in the success rate of greedy routing (tessellation G_{711}). Average and median computed conditionally on change. P-values for Wilcoxon paired tests.

Figure 3: Density of L_2/L_g (black) and L_7/L_g (blue) for $T = 0.7$.

Wilcoxon paired tests with the alternative hypotheses that the success rate is lower after the discretization are always 0.00). The whole procedure improves the results in more than 45% of cases, however the change for bigger graphs is not statistically significant (p-values for paired Wilcoxon tests with the alternative hypotheses that the success rates increased after our procedure are greater than 10%). For large graphs (over 4000 vertices) in about half of the cases the success rate after the procedure is not worse than the original one.

To reduce the negative effect of discretization, we also perform the same experiment using the G_{711} grid. The results are shown in Table 7. Contrary to the G_{710} tessellation, usage of the finer tessellation for routing (when all three steps are performed) improves the success rate, and the effect is statistically significant. The general directions of the effects resemble the case of coarser grid. Discretization leads to a statistically significant decrease in the success rate; the bigger graphs, the less frequent a noticeable deterioration.

5.3 Changing the temperature

Real-world graphs are considered to have larger temperature T . We have also experimented with changing the temperature T to 0.7. This value of T has been used for mapping the Internet [BPK10].

For $T = 0.7$, the embedder and local search actually tend to achieve a better result than the groundtruth. For all sizes of graphs, we observe about 3% improvement in the absolute value of log-likelihood on average ($1 - L_2/L_7$)

n	deterioration (discretization)			improvement (local search)			improvement (three steps)			
	%	med	avg	%	med	avg	%	med	avg	p-value
300	99.9	3.88	4.53	88.5	2.27	2.72	60.7	1.04	1.37	0.00
500	100.0	3.60	4.26	88.6	1.74	2.15	59.4	0.84	1.11	0.00
1000	100.0	3.39	3.73	88.1	1.25	1.48	55.9	0.65	0.78	0.00
2000	100.0	3.21	3.47	87.7	0.99	1.15	52.9	0.46	0.59	0.02
3000	100.0	2.87	3.00	84.4	0.72	0.84	46.7	0.30	0.42	0.98
4000	100.0	3.22	3.31	89.7	0.80	0.88	38.3	0.28	0.37	1.00
5000	100.0	2.98	3.02	88.6	0.63	0.69	36.1	0.19	0.24	1.00
10000	100.0	2.95	2.96	90.6	0.55	0.60	29.1	0.13	0.22	1.00
15000	100.0	3.23	3.23	95.5	0.73	0.75	24.4	0.12	0.16	1.00

Table 8: Changes in the success rate of greedy routing (tessellation G_{710} , $T = 0.7$). Average and median computed conditionally on change. P-value for Wilcoxon paired test.

(Figure 3). This effect is statistically significant (p-values for paired Wilcoxon tests with alternative hypotheses that the values of log-likelihood increased after our procedure always 0.00).

One could argue that the temperature plays critical role for the success of the greedy routing. With a higher temperature, the links are less predictable, and thus we can expect a lower success rate. We conducted the simulations to check if the insights change in the case of the value of temperature more typical to real-world networks. Table 8 contains the results of the experiments with respect to the size of the graph.

Our insights driven from simulations for $T = 0.7$ resemble the conclusions for the case of $T = 0.1$. In the case of the coarse tessellation (Table 8) the possibility of improvement depends on n . For small and medium-sized graphs the effect is statistically significant; the larger the graph, the less probable statistically significant improvement (p-values of Wilcoxon paired test greater than any conventional significance levels). With the finer tessellation (Table 9), no matter the size of the graph, the post-procedure improvement is statistically significant (p-values for paired Wilcoxon tests with the alternative hypothesis that the success rate increased after our procedure are always 0.00).

We also checked if the change of the tessellation significantly improves the success rate. To this end, we performed paired Wilcoxon tests with the alternative hypotheses that the success rate increased after using a finer tessellation. In all the cases, the p-values were 0.00, so the effect of the tessellation is statistically significant.

6 Conclusion

We introduced the discrete version of the HRG model, which allows efficient algorithms while avoiding numerical issues. We also presented the result of the

n	deterioration (discretization)			improvement (local search)			improvement (three steps)		
	%	med	avg	%	med	avg	%	med	avg
300	98.3	1.86	2.25	81.1	1.56	1.90	63.5	1.00	1.32
500	99.5	1.81	2.14	85.9	1.30	1.57	68.1	0.94	1.12
1000	99.9	1.65	1.86	84.0	0.97	1.11	67.5	0.62	0.75
2000	100.0	1.61	1.71	87.1	0.75	0.83	67.3	0.44	0.55
3000	100.0	1.40	1.48	83.4	0.53	0.61	64.1	0.32	0.21
4000	100.0	1.61	1.64	90.5	0.56	0.62	61.7	0.28	0.36
5000	100.0	1.48	1.50	88.8	0.45	0.49	59.5	0.25	0.28
10000	100.0	1.47	1.48	94.1	0.41	0.46	61.0	0.18	0.22
15000	100.0	1.61	1.61	98.4	0.53	0.53	65.1	0.17	0.19

Table 9: Changes in the success rate of greedy routing (tessellation G_{711} , $T = 0.7$). Average and median computed conditionally on change.

experimental evaluation of this model. We analyzed both the real-world networks and 20,000 artificial ones, paying special attention to the possible application of the model in greedy routing. Our experimental evaluation shows that we achieve a good approximation of log-likelihood in the HRG model and that using local search significantly improves its log-likelihood, even when converting back to HRG. This is visible both in real-world and in simulated networks. A similar procedure also slightly improves the success rate of greedy routing when a sufficiently fine tessellation is used. The choice of the tessellation seems to be crucial for the success rate for all tested values of the parameters.

This work has been supported by the National Science Centre, Poland, grant DEC-2016/21/N/HS4/02100.

References

- [BA99] Albert-Laszlo Barabasi and Reka Albert. Emergence of scaling in random networks. *Science*, 286(5439):509–512, 1999.
- [BFKK18] Thomas Bläsius, Tobias Friedrich, Maximilian Katzmann, and Anton Krohmer. Hyperbolic embeddings for near-optimal greedy routing. In *Algorithm Engineering and Experiments (ALENEX)*, pages 199–208, 2018.
- [BFKL16] Thomas Bläsius, Tobias Friedrich, Anton Krohmer, and Sören Laue. Efficient embedding of scale-free graphs in the hyperbolic plane. In *European Symposium on Algorithms (ESA)*, pages 16:1–16:18, 2016.

- [BKL18] Karl Bringmann, Ralph Keusch, and Johannes Lengler. Geometric inhomogeneous random graphs. *Theoretical Computer Science*, 2018.
- [BPK10] Marián Boguñá, Fragkiskos Papadopoulos, and Dmitri Krioukov. Sustaining the internet with hyperbolic mapping. *Nature Communications*, 1(6):1–8, Sep 2010.
- [Bö74] Károly Böröczky. Gömbkitöltések állandó görbületű terekben I. *Matematikai Lapok*, 25:265–306, 1974.
- [Cel16] Dorota Celińska. Information and influence in social network of Open Source community. In *9th Annual Conference of the EuroMed Academy of Business*, 2016.
- [CFK⁺97] James W. Cannon, William J. Floyd, Richard Kenyon, Walter, and R. Parry. Hyperbolic geometry. In *In Flavors of geometry*, pages 59–115. University Press, 1997. Available online at <http://www.msri.org/communications/books/Book31/files/cannon.pdf>.
- [Gou13] Georgios Gousios. The ghtorrent dataset and tool suite. In *Proceedings of the 10th Working Conference on Mining Software Repositories*, MSR '13, pages 233–236, Piscataway, NJ, USA, 2013. IEEE Press.
- [GPP12] Luca Gugelmann, Konstantinos Panagiotou, and Ueli Peter. Random hyperbolic graphs: Degree sequence and clustering. In Artur Czumaj, Kurt Mehlhorn, Andrew Pitts, and Roger Wattenhofer, editors, *Automata, Languages, and Programming*, pages 573–585, Berlin, Heidelberg, 2012. Springer Berlin Heidelberg.
- [Gri12] Ilya Grigorik. Github Archive. <https://www.githubarchive.org/>, 2012.
- [KCK21] Eryk Kopczyński and Dorota Celińska-Kopczyńska. RogueViz: non-Euclidean geometry engine for visualizations, games, math art, and research, Oct 2021. <https://github.com/zenorogue/hyperrogue/>.
- [KCv17] Eryk Kopczyński, Dorota Celińska, and Marek Čtrnáct. HyperRogue: Playing with hyperbolic geometry. In *Proceedings of Bridges : Mathematics, Art, Music, Architecture, Education, Culture*, pages 9–16, Phoenix, Arizona, 2017. Tessellations Publishing.
- [KW04] Stephen G. Kobourov and Kevin Wampler. *Non-euclidean spring embedders*, pages 207–214. 2004.
- [LK14] Jure Leskovec and Andrej Krevl. SNAP Datasets: Stanford large network dataset collection. <http://snap.stanford.edu/data>, June 2014.

- [LRP95] John Lamping, Ramana Rao, and Peter Pirolli. A focus+context technique based on hyperbolic geometry for visualizing large hierarchies. In *Proceedings of the SIGCHI Conference on Human Factors in Computing Systems*, CHI '95, pages 401–408, New York, NY, USA, 1995. ACM Press/Addison-Wesley Publishing Co.
- [Mun98] Tamara Munzner. Exploring large graphs in 3d hyperbolic space. *IEEE Computer Graphics and Applications*, 18(4):18–23, 1998.
- [PAK15] Fragkiskos Papadopoulos, Rodrigo Aldecoa, and Dmitri Krioukov. Network geometry inference using common neighbors. *Phys. Rev. E*, 92:022807, Aug 2015.
- [PKS⁺12] Fragkiskos Papadopoulos, Maksim Kitsak, M. Angeles Serrano, Marian Boguñá, and Dmitri Krioukov. Popularity versus Similarity in Growing Networks. *Nature*, 489:537–540, Sep 2012.
- [SDSGR18] Frederic Sala, Chris De Sa, Albert Gu, and Christopher Re. Representation tradeoffs for hyperbolic embeddings. In *Proc. ICML*, pages 4460–4469, Stockholmsmässan, Stockholm Sweden, 2018. PMLR.
- [SJ19] Zeynab Samei and Mahdi Jalili. Application of hyperbolic geometry in link prediction of multiplex networks. *Scientific Reports*, 9(1):12604, Aug 2019.
- [vLMP15] Moritz von Looz, Henning Meyerhenke, and Roman Prutkin. *Generating Random Hyperbolic Graphs in Subquadratic Time*, pages 467–478. Springer Berlin Heidelberg, Berlin, Heidelberg, 2015.